Searching for $\mu \to e\gamma$ with MEG

G. Cavoto ([1])

([1]) *Istituto Nazionale di Fisica Nucleare, Sezione di Roma*
Piazzale A.Moro,2 00185 Roma, Italy

Summary. — New results of a search for the ultra-rare decay $\mu \to e\gamma$ by the MEG collaboration at the Paul Scherrer Institut (PSI) continuous muon beam are reported here. The data were taken during 2009 and 2010 and correspond to approximately $1.8\ 10^{14}$ muon stopped on target. A maximum likelihood fit analysis sets an upper limit at 90% C.L. on the branching ratio, $\mathcal{B}(\mu \to e\gamma) < 2.4\ 10^{-12}$, the best limit ever achieved for this process.

PACS 13.35.Bv – Decays of muons.
PACS 11.30.Hv – Flavor symmetries.
PACS 12.10.Dm – Unified theories and models of strong and electroweak interactions.

1. – Description

Standard model of elementary particles (SM) forbids processes with violation of the lepton flavour accidental symmetry (LFV). The process $\mu \to e\gamma$ is highly suppressed even with the introduction of neutrino masses and mixing in the SM [1, 2]. An immeasurably small branching ratio ($\mathcal{B} \lesssim 10^{-51}$) for this decay would be allowed. On the contrary, new physics scenarios beyond SM, such as supersymmetric grand unified theories or theories with extra dimensions, predict branching ratios in the 10^{-12} to 10^{-14} range [3, 4, 5]. This is close to the present limit set by the MEGA experiment [6], $\mathcal{B} \leq 1.2 \times 10^{-11}$, which places one of the most stringent constraints on the formulation of such theories. Observation of $\mu \to e\gamma$ therefore would be an unambiguous signature of new physics, while improvements on the existing limit would stringently constrain many of the new physics scenarios beyond SM.

2. – The MEG experiment

$\mu \to e\gamma$ process has simple two-body kinematics with well defined photon and positron energies. An experiment devoted to search for this process should be carefully optimized

to fight the background by obtaining the best experimental resolution with some trade-off on the detection efficiency. Positive muons are not captured on target nuclei and they must be preferred for this search. The background to $\mu^+ \to e^+\gamma$ decay comes either from radiative muon decays $\mu^+ \to e^+\nu\bar{\nu}\gamma$ (RMD) in which the neutrinos carry away little energy or from an accidental coincidence of an energetic positron from a normal Michel decay with a $\gamma-$ray coming from RMD, Bremsstrahlung or positron annihilation-in-flight. The accidental coincidences are by more than one order of magnitude the dominant background. Given the possibly tiny $\mathcal{B}$ value a high beam rate is necessary. The PSI πE5 beam line is used to stop 3×10^7 positive muons per second in the target. The residual polarization of the decaying muons along the beam axis was measured to be $\langle P \rangle = -0.89 \pm 0.04$.

The MEG detector [7, 8] provides an asymmetric coverage (10% solid angle in total) of the thin muon stopping target (205 μm-thick polyethylene) in order to minimize the material crossed by the photon before being detected. It is composed of a positron spectrometer and a photon detector in search of back-to-back and time coincident photons and positrons. The positron spectrometer consists of a set of drift chambers (DC) [9] and scintillation timing counters (TC) [10] located inside a superconducting solenoid with a gradient field [11] along the beam axis, ranging from 1.27 Tesla at the centre to 0.49 Tesla at either end. Such B field efficiently sweeps out the low energy positrons from the spectrometer volume. The photon detector [12], located outside of the solenoid, is a homogeneous volume (900 ℓ) of liquid xenon (LXe) viewed by 846 UV-sensitive photo-multiplier tubes (PMTs) submerged in the liquid. The spectrometer measures the positron momentum vector and timing, while the LXe detector is used to reconstruct the $\gamma-$ray energy as well as the position and time of its first interaction in LXe. All the signals are individually digitized by in-house designed waveform digitizers based on the multi-GHz domino ring sampler chip (DRS) [13].

The MEG detector response, resolutions and stability are constantly monitored and calibrated. The PMTs of the LXe detector are calibrated by LEDs and α-sources immersed in the liquid [14] during physics data acquisition. The energy scale and resolutions of the LXe detector are measured over the energy range of 4.43 to 129.4 MeV using various $\gamma-$rays sources. Photons from a radioactive Am/Be source and from (p,γ)-reaction using a dedicated Cockcroft-Walton accelerator (CW) [15] are injected twice a week in the LXe detector, while once a year a $\pi^- p$ charge exchange and radiative capture reactions (CEX) are used to produce monochromatic photons in an energy range very close to the signal photon energy. A 9 MeV-γ line from the capture in nickel of neutrons from a pulsed and triggerable deuteron-deuteron neutron generator allows to check the stability of the LXe detector even during data-taking. The relative time between the TC and LXe detector is monitored using RMD and 2γ-events from ${}^{11}_{5}\mathrm{B}(p,2\gamma){}^{12}_{6}\mathrm{C}$ reactions.

The $\mu^+ \to e^+\gamma$ trigger requires the presence of a high energy $\gamma-$ray in the LXe detector and a hit on the timing counters within a 20 ns window together with an approximate back-to-back topology. Pre-scaled monitoring and calibration triggers are also recorded. A more detailed description of the MEG detector can be found in Ref. [8].

3. – Data analysis

The results presented here are based on data collected in 2009 and 2010 (for a total of 1.8×10^{14} μ^+-decays in the target). The 2010 statistics are about twice that of 2009. All sub-detectors were running stably during these periods.

In 2010 a DRS upgrade resulted in an improvement in the time resolution while an

increase in noise in the DC, due to a deterioration of the HV power supplies, and some unusable DC modules caused a slightly worse positron tracking performances.

A blind analysis procedure was adopted such that events close to the signal region were kept hidden (blind region) until all the analysis procedures had been completely defined. A maximum likelihood analysis fit method was used to extract the signal and background yields. Therefore, the probability density functions (PDFs) needed for the likelihood analysis were constructed using the only events outside of the blind region (side-bands) or calibration samples.

3˙1. *Observables reconstruction and resolutions.* – The kinematic variables used to identify the $\mu^+ \to e^+\gamma$ decays are the γ-ray and e^+ energies (E_γ, E_e), their relative directions ($\theta_{e\gamma}$, $\phi_{e\gamma}$) and relative emission time ($t_{e\gamma}$). The relative directions are defined as $\theta_{e\gamma} = (\pi - \theta_e) - \theta_\gamma$ and $\phi_{e\gamma} = (\pi + \phi_e) - \phi_\gamma$, θ and ϕ being the polar angle and the azimuthal angle, respectively, taking the z-axis as the beam-axis. The offline event selection requires at least one e^+-track reconstructed in the spectrometer and pointing to the target, with minimal quality cuts applied. The blind region is defined by $48 < E_\gamma < 58$ MeV and $|t_{e\gamma}| < 1$ ns.

The positron track reconstruction in the spectrometer is based on a Kalman filter technique [16]. Effects of multiple scattering and energy loss in the detector materials in the presence of the non-uniform magnetic field are taken into account. The gradient magnetic field was measured with Hall probes in 2006 and compared with the prediction from the coil currents showing good agreement (within 0.2%). Only the major component along the beam axis of the measured field is used in the analysis to avoid possible misalignment errors from the Hall probes. The other minor components are deduced from Maxwell equations with boundary conditions at a symmetry plane at the magnet centre. Internal alignment of the DC is obtained by tracking cosmic ray muons without a magnetic field and by minimizing the measured residuals in a manner independent of the initially assumed alignment [17]. The absolute position of the DC system is based on an optical survey.

The resolutions of the positron track direction are estimated by exploiting tracks with two full turns in the DC sensitive volume Each turn is treated as an independent sub-track and the resolutions are extracted from the difference between the fitted parameters of the two reconstructed sub-tracks. MonteCarlo (MC) simulations demonstrates that the RMS of such differences (fig.1) are good estimates of the angular resolutions at the target. Small corrections (at the level of 10%) account for a dependence on positron momentum.

The reference energy resolution is evaluated by fitting the kinematic edge of the Michel decays with a convolution of the theoretical Michel spectrum with a resolution function represented by a sum of three Gaussians. The core Gaussian component describes about 80% of the events with a tail ($\sigma_{tail} = 3\sigma_{core}$) and an outlier ($\sigma_{out} = 6\sigma_{core}$) components being approximately 15% and 5% of the total.

The decay vertex coordinates and the positron direction at the vertex are determined by extrapolating the reconstructed track back to the target with the constraint given by the target plane. Given this constraint, a geometrical correlation is generated between ϕ_e at the vertex position and E_e, that can be parametrized as $\sigma_{\phi_e} = \sqrt{\sigma_0^2 + (k \tan \phi_e)^2}$ where σ_0 is the ϕ_e resolution for $\phi_e = 0$, *i.e.* the direction orthogonal to the target plane, and $k \sim 10$ mrad is a parameter that can be determined experimentally by using the two-turn method. This effect is perfectly reproduced by the MC simulation.

The resolution on the decay vertex coordinates is also determined by the two-turn

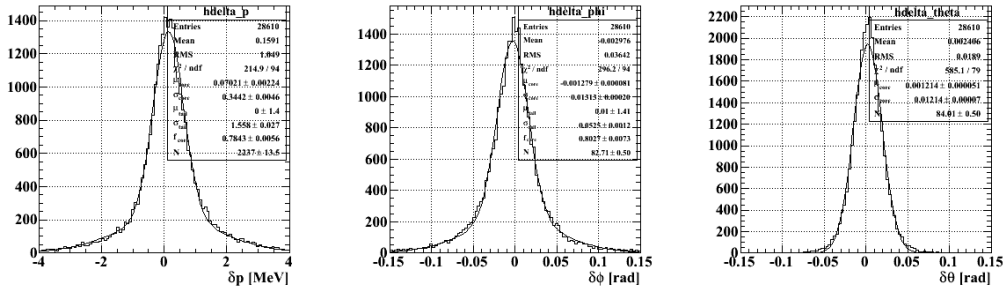

Fig. 1. – Double turn tracks momentum (left) and angle (center and right) distribution. The plots shows the difference of the sub-tracks parameters, obtained with independent fits to each sub-track.

method; along the beam axis it is described by a Gaussian while in the vertical direction it is described by the sum of two Gaussians (core component approximately 85%).

The determination of the photon energy E_γ in the LXe detector is based on the sum of the number of scintillation photons detected by the PMTs; correction factors take into account the different PMT geometrical acceptances. Due to its geometry the detector response is not totally uniform over the photon entrance window; this is corrected for by using γ-lines from CW and CEX reactions. The absolute energy scale and resolution at the signal energy $E_\gamma = 52.8\,\mathrm{MeV}$ are determined by the CEX measurement; the resolution σ_R, extracted from a Gaussian fit to the high energy side of the spectrum, depends also on the depth (w) of the $\gamma-$ray conversion point from the photon entrance surface of the LXe detector. Events with shallow conversion point ($w < 2\,\mathrm{cm}$) represents the 37% of the total and have a resolution about 20% worse than the events with $w > 2\,\mathrm{cm}$. The 3D-map of the measured resolutions is incorporated into the PDFs for the likelihood analysis.

The photon energy scale and the resolutions are cross-checked by fitting the background spectra measured in the side-bands with the theoretical RMD spectrum folded with the detector resolutions. This allows to monitor the resolutions during the run and confirms that they are well represented by the CEX evaluations. The systematic uncertainty of the E_γ-scale is estimated to be $\simeq 0.3\%$.

Since MEG operates at a high beam intensity, it is important to recognize and unfold pile-up photons. For each event the spatial and temporal distributions of the PMT charge are studied to identify photon pile-up in the LXe detector; in case of positive identification, corrections to the PMT charges are applied. Cosmic ray events are rejected using their topological characteristics.

The position of the first interaction of the γ-ray in the LXe detector is derived from the light distribution measured by the PMTs close to the region of the energy deposition by fitting the distribution with the expectation. The position resolution in the plane of the photon entrance window is measured in a dedicated CEX run with a lead slit-collimator placed in front of the LXe detector, while the w resolution and the position dependence of the resolutions are evaluated by a MC simulation.

The γ-ray direction (θ_γ and ϕ_γ) is defined by the line connecting the decay vertex to the γ-ray conversion point measured by the LXe detector.

The relative time $t_{e\gamma}$ is derived from the two time measurements by the LXe detector

and the TC, after correcting for the length of the particles flight-paths. The associated resolutions at the signal energy are evaluated from the RMD peak observed in the E_γ side-band; a small correction takes into account the E_γ-dependence measured in the CEX calibration runs. The position of the RMD-peak corresponding to $t_{e\gamma} = 0$ was monitored constantly during the physics data-taking period and found to be stable to within 15 ps.

All the mentioned resolutions are collected in tab.I for 2009 and 2010 data separately. Reconstruction efficiency for positron and photon within the detector acceptance are also reported in tab.I .

TABLE I. – *Resolution (Gaussian σ) and efficiencies for 2009 and 2010 data*

PDF parameters	2009	2010
core $\frac{\sigma_{E_{e^+}}}{E_{e^+}}$	0.74%	0.74%
Core Gaussian fraction	83%	79%
e^+ σ_θ	9.4 mrad	11.0 mrad
e^+ σ_ϕ (ϕ=0)	6.7 mrad	7.2 mrad
e^+ σ_Z / $\sigma_Y(core)$	1.5/1.1mm	2.0/1.1 mm
$\frac{\sigma_{E_\gamma}}{E_\gamma}$ w>2 cm	1.9%	1.9%
γ position at LXe $\sigma_{(u,v)}$-σ_w	5-6 mm	5-6 mm
$\theta_{e\gamma}$	14.5 mrad	17.1 mrad
$\phi_{e\gamma}$	13.1 mrad	14.0 mrad
γ-e^+ timing	150 ps	130 ps
Efficiency		
trigger	91%	92%
γ reconstruction	58%	59%
e^+ reconstruction	40%	34%

3·2. *Maximum likelihood analysis.* – A likelihood analysis is carried out for events in a portion of the blind region (analysis region) defined by $48 < E_\gamma < 58\,\mathrm{MeV}$, $50 < E_e < 56\,\mathrm{MeV}$, $|t_{e\gamma}| < 0.7\,\mathrm{ns}$, $|\theta_{e\gamma}| < 50\,\mathrm{mrad}$ and $|\phi_{e\gamma}| < 50\,\mathrm{mrad}$. These intervals in the analysis variables are between five and twenty sigmas wide to fully contain the signal events and also retain some background events. The best estimates of the numbers of signal, RMD and accidental background (BG) events in the analysis region are obtained by maximizing the following likelihood function:

$$\mathcal{L}\left(N_{\mathrm{sig}}, N_{\mathrm{RMD}}, N_{\mathrm{BG}}\right) = \frac{e^{-N}}{N_{\mathrm{obs}}!} e^{-\frac{(N_{\mathrm{RMD}}-\langle N_{\mathrm{RMD}}\rangle)^2}{2\sigma^2_{\mathrm{RMD}}}} e^{-\frac{(N_{\mathrm{BG}}-\langle N_{\mathrm{BG}}\rangle)^2}{2\sigma^2_{\mathrm{BG}}}} \times \prod_{i=1}^{N_{\mathrm{obs}}} \left(N_{\mathrm{sig}} S(\vec{x}_i) + N_{\mathrm{RMD}} R(\vec{x}_i) + N_{\mathrm{BG}} B(\vec{x}_i)\right),$$

where $\vec{x_i} = \{E_\gamma, E_e, t_{e\gamma}, \theta_{e\gamma}, \phi_{e\gamma}\}$ is the vector of observables for the i-th event, N_{sig}, N_{RMD} and N_{BG} are the fitted numbers of signal, RMD and BG events, while S, R and B are their corresponding PDFs. $N = N_{\mathrm{sig}} + N_{\mathrm{RMD}} + N_{\mathrm{BG}}$ and N_{obs} is the observed

total number of events in the analysis window. $\langle N_{\rm RMD}\rangle (= 27.2(52.2))$ and $\langle N_{\rm BG}\rangle (= 270.9(610.8))$ are the numbers of RMD and BG events extrapolated from the side-bands together with their uncertainties $\sigma_{\rm RMD} (= 2.8(6.0))$ and $\sigma_{\rm BG} (= 8.3(12.6))$, respectively for 2009(2010) data.

The signal PDF $S(\vec{x_i})$ is the product of the PDFs for E_e, $\theta_{e\gamma}$, $\phi_{e\gamma}$ and $t_{e\gamma}$, which are correlated variables, as explained above, and the E_γ PDF. The PDFs properly incorporate the measured resolutions and correlations among $E_e, \theta_{e\gamma}$, $\phi_{e\gamma}$ and $t_{e\gamma}$ on an event-by-event basis. The RMD PDF $R(\vec{x_i})$ is the product of the same $t_{e\gamma}$-PDF as that of the signal and the PDF of the other four correlated observables, which is formed by folding the theoretical spectrum with the detector response functions. The BG PDF $B(\vec{x_i})$ is the product of the five PDFs, each of which is defined by the single background spectrum, precisely measured in the side-bands. The dependence of the resolutions on the position of the γ-ray interaction point and on the positron tracking quality is taken into account in the PDFs.

A frequentist approach with a profile likelihood-ratio ordering [18, 19] is used to compute the confidence intervals on $N_{\rm sig}$. Other, independent analysis schemes based on averaged PDFs without event-by-event information or Bayesian approach were also used and found to be compatible with the analysis presented here to within 10 to 20% difference in the obtained branching ratio upper limits.

In order to convert $N_{\rm sig}$ into a branching ratio value the normalization relative to the Michel decay is computed [8] by counting the number of Michel positrons passing the same analysis cuts. This is accomplished by means of a pre-scaled Michel positron trigger enabled during the physics data-taking. A correction to the pre-scaling factor due to positron pile-up in the TC is taken into account. Another method for computing the normalization uses RMD events in the E_γ side-band and the theoretical branching ratio of the RMD. The normalizations calculated by these two independent methods are in good agreement and are combined to give the normalization factor with a 7% uncertainty.

The sensitivity ($\mathcal{S}$) of the experiment with a null signal hypothesis is evaluated by taking the median of the distribution of the upper limit on the branching ratio obtained over an ensemble of toy MC experiments. The rates of RMD and BG events, as measured in the side-bands, are assumed in the simulated experiments. In fig.2 the distribution of the upper limit on $N_{\rm sig}$ on these ensembles are reported for the 2009 and 2010 data sets separately. It must be emphasized that these sensitivities are consistent with the upper limits obtained by the likelihood analyses in several comparable analysis regions of the $t_{e\gamma}$ side-bands demonstrating a good control over the background description.

After calibrations, optimization of the analysis algorithms and background studies in the side-bands are completed, the likelihood analysis in the analysis region is performed. In fig. 3 the event distribution for the various observables is shown with the superimposed PDF.

The analysis of the full data sample gives a 90% C.L. upper limit of 2.4×10^{-12} on $\mathcal{B}$ $(\mu \to e\gamma)$. The 90% C.L. intervals as well as the best estimate of the branching ratio for 2009 and 2010 data separately are also given in tab. II. The 2009 data set, which gives a positive best estimate for the branching ratio, is consistent with the hypothesis $\mathcal{B} = 0$ with an 8% probability.

The systematic uncertainties for the parameters of the PDFs and the normalization factor are taken into account in the calculation of the confidence intervals by fluctuating the PDFs according to the uncertainties. The largest contributions to the systematic uncertainty, which amount to a shift of about 2% in total in the branching ratio upper limit, come from the uncertainties of the offsets of the relative angles, the correlations in

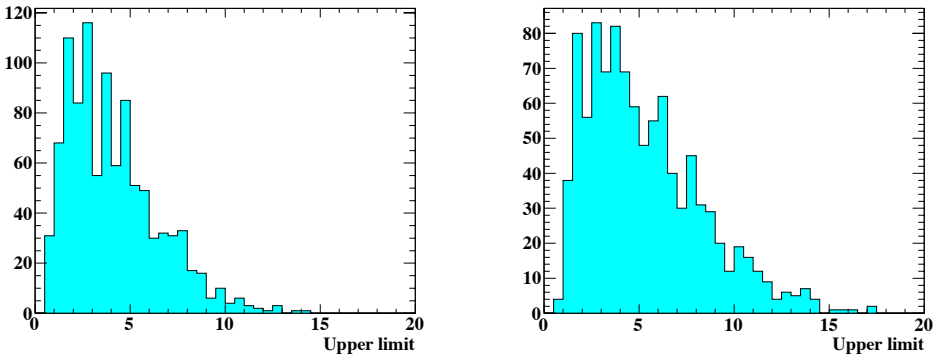

Fig. 2. – Distribution of 90% upper limit on $N_{\rm sig}$ in two ensemble of toy MC experiments corresponding to 2009 (left) and 2010 (rigth) dataset.

the positron observables and the normalization.

4. – Conclusions and Perspectives.

In this contribution the results of 2009 and 2010 data analysis collected by the MEG experiment has been presented, leading to a 90% C.L. upper limit of 2.4×10^{-12} on $\mathcal{B}$

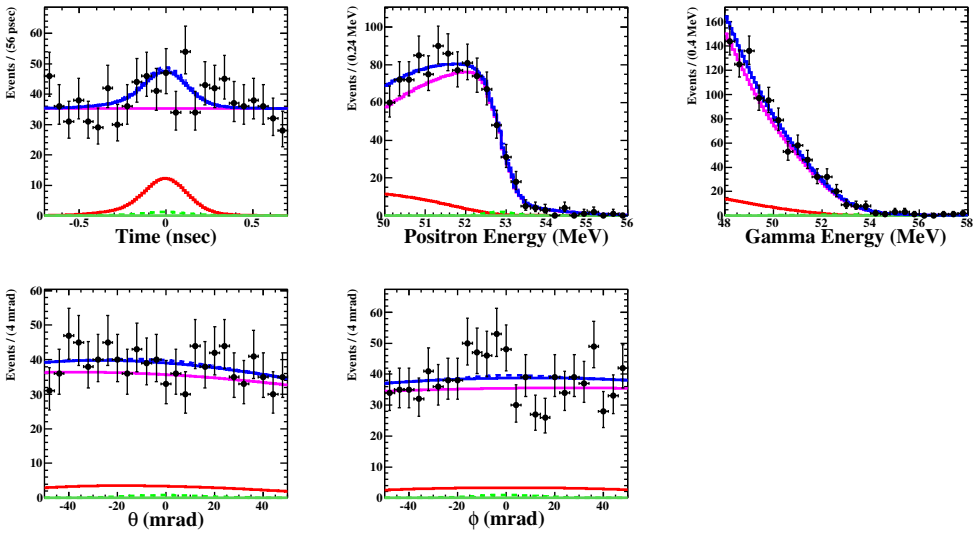

Fig. 3. – Distributions of events for the various observables, $t_{e\gamma}$, E_e, and E_γ on the top row, $\theta_{e\gamma}$ and $\phi_{e\gamma}$ on the bottom row. The projected PDF total, S, R and B (blue, green, red, and magenta) are superimposed. The dotted lines includes the 90 % UL on $N_{\rm sig}$ for comparison.

TABLE II. – *Single event sensitivity (SES), sensitivity ($\mathcal{S}$), best fit ($\mathcal{B}_{fit}$),and upper limits (UL) at the 90% C.L. of the branching ratio (given in $\times 10^{-12}$ unit) for the 2009, 2010 and combined 2009 + 2010 data sets. Best fit ($N_{\rm sig}$) events and $N_{\rm obs}$ are also reported.*

Data set	SES	$\mathcal{S}$	$N_{\rm obs}$	$N_{\rm sig}$	$\mathcal{B}_{\rm fit}$	UL
2009	0.9	3.3	311	3.4	3.2	9.6
2010	0.4	2.2	645	-2.2	-1.0	1.7
2009 + 2010	–	1.6	–	–	-0.2	2.4

($\mu \to e\gamma$), which constitutes the most stringent limit on the existence of the $\mu \to e\gamma$ decay, superseding the previous limit by a factor of 5. In 2011 the MEG experiment has already doubled the collected data and plans to add more data in 2012. The detector performances are expected to be similar. The predicted sensitivity at the end of 2012 would be in the range 10^{-13} challenging several model of new physics. An upgrade of the system is under discussion and could further bring down the sensitivity to less than 10^{-13}.

5. – Acknowledgements

The author thanks his collaborators of the MEG experiment. He acknowledges the support of INFN (Italy).

REFERENCES

[1] T. P. Cheng, L. -F. Li, Phys. Rev. Lett. **45** (1980) 1908.
[2] R. Barbieri, L. J. Hall, Phys. Lett. **B338** (1994) 212-218. [hep-ph/9408406].
[3] R. Barbieri, L. Hall and A. Strumia, Nucl. Phys. B **455** (1995) 219.
[4] J. Hisano, D. Nomura and T. Yanagida, Phys. Lett. B **437** (1998) 351.
[5] M. Raidal *et al.*, Eur. Phys. J. C **57** (2008) 13.
[6] M. L. Brooks *et al.* [MEGA Collaboration], Phys. Rev. Lett. **83**, (1999) 1521.
[7] A. Baldini, T. Mori *et al.*, "The MEG experiment: search for the $\mu \to e\gamma$ decay at PSI", available at `http://meg.psi.ch/docs`.
[8] J. Adam *et al.* [MEG collaboration], Nucl. Phys. B **834** (2010) 1.
[9] M. Hildebrandt *et al.* [MEG collaboration], Nucl. Instr. and Meth. **A623** (2010) 111.
[10] M. De Gerone *et al.*, Nucl. Instr. and Meth. **A638** (2010) 41.
[11] W. Ootani *et al.*, IEEE Trans. Applied Superconductivity **14** (2004) 568.
[12] S. Mihara *et al.* [MEG Collaboration], J. Phys.: Conf. Ser. **308**(2011)012009.
[13] S. Ritt *et al.*, Nucl. Instr. and Meth. **A623** (2010) 486.
[14] A. Baldini *et al.*, Nucl. Instr. and Meth. **A565** (2006) 589.
[15] J. Adam *et al.* [MEG collaboration], Nucl. Instr. and Meth. **A641** (2011) 19.
[16] R. Frühwirt, *et al.* "Data Analysis Techniques for High Energy Physics", second ed. (Cambridge University Press, Cambridge, 2000).
[17] CMS collaboration, JINST **5** (2010) T03009.
[18] K. Nakamura et al. (Particle Data Group), J. Phys. **G** 37 (2010) 075021.
[19] G. J. Feldman and R. D. Cousins, Phys. Rev D **57**, (1998) 3873.